

Stiffness of the C-terminal disordered linker affects the geometry of the active site in endoglucanase Cel8A

Bartosz Różycki,^{*a} and Marek Cieplak^a

Cellulosomes are complex multi-enzyme machineries which efficiently degrade plant cell-wall polysaccharides. The multiple domains of the cellulosome proteins are often tethered together by intrinsically disordered regions. The properties and functions of these disordered linkers are not well understood. In this work, we study endoglucanase Cel8A, which is a relevant enzymatic component of the cellulosomes of *Clostridium thermocellum*. We use both all-atom and coarse-grained simulations to investigate how the equilibrium conformations of the catalytic domain of Cel8A are affected by the disordered linker at its C terminus. We find that when the endoglucanase is bound to its substrate, the effective stiffness of the linker can influence the distances between groups of amino-acid residues throughout the entire enzymatic domain. In particular, variations in the linker stiffness can lead to small changes in the geometry of the active-site cleft. We suggest that such geometrical changes may, in turn, have an effect on the catalytic activity of the enzyme.

1 Introduction

Cellulosomes are large, multi-enzyme complexes that are found on the surfaces of different cellulolytic microorganisms^{1,2}. Their function is degradation of plant cell-wall polysaccharides to simple sugars^{2,3}. One of the major challenges in the current research on the cellulosomes is to understand how their molecular architectures and activities are related^{3,4}. Importantly, the structural characterization of the cellulosome complexes can provide a platform for biotechnological and nanotechnological applications, including prospects for producing biofuels from plant-cell-wall biomass³.

The multiple proteins of cellulosomes are composed of numerous functional domains, which interact with each other and with polysaccharides. These domains are usually tethered to one another by intrinsically disordered polypeptide segments, which are commonly called linkers. Interestingly, a number of distinct multi-domain proteins and protein complexes belonging to cellulosomes of different cellulolytic microorganisms have been found to be highly flexible in solution^{5–8}. Their flexibility seems to be needed for the simultaneous binding of the multiple enzymatic domains to plant cell-wall polysaccharides. A likely role of the disordered linkers is thus to provide the required degree of flexibility while maintaining the integrity of the cellulosome complexes.

The intrinsically disordered linkers in cellulosome complexes differ significantly in amino-acid sequence and length – from several to about a hundred amino-acid residues. The reasons for this

variability among the cellulosomal linkers have been a puzzle so far. As a matter of fact, the biological functions of the disordered linkers are not well understood. It has been demonstrated that the sequential length of linkers can influence the enzymatic activity of designer cellulosomes⁴ but in some cases this effect is marginal⁹. However, the relations between the physical properties of the disordered linkers and the enzymatic activity of the cellulosomes remain unknown. Here, we study endoglucanase Cel8A of *Clostridium thermocellum* and show that effective stiffness of the disordered linker at the C-terminus of the catalytic domain has an impact on the geometry of the active-site region when Cel8A is bound to its substrate. Such geometrical changes may in turn influence the catalytic activity of the enzyme.

A kinetic model for a two-domain cellulase, which treats the catalytic domain (CD) and the carbohydrate-binding module (CBM) as two random walkers in one dimension, predicts that the cooperative action of the CD and CBM domains depends on the length and stiffness of the linker between CD and CBM¹⁰. This model is quite general and does not make use of structural information about the cellulase. In contrast, our study is based on the atomic structure of the catalytic domain of endoglucanase Cel8A, and gives predictions about the structural rearrangements within the enzyme. We use coarse-grained models in which amino-acid residues are represented as single beads, and investigate how the near-native conformations of the CD in Cel8A are affected by the stiffness of the disordered linker at its C terminus. The predictions of the coarse-grained model are corroborated by all-atom simulations.

The use of thermostable cellulosomes is advantageous for the breakdown of cellulosic biomass toward the commercial production of biofuels. For this reason, experimental and bioinformatics-

^a Institute of Physics, Polish Academy of Sciences, Al. Lotników 32/46, 02-668 Warsaw, Poland

* Tel: 48 22 116 3265; E-mail: rozycki@ifpan.edu.pl

† Electronic Supplementary Information (ESI) available: []. See DOI: 10.1039/b000000x/

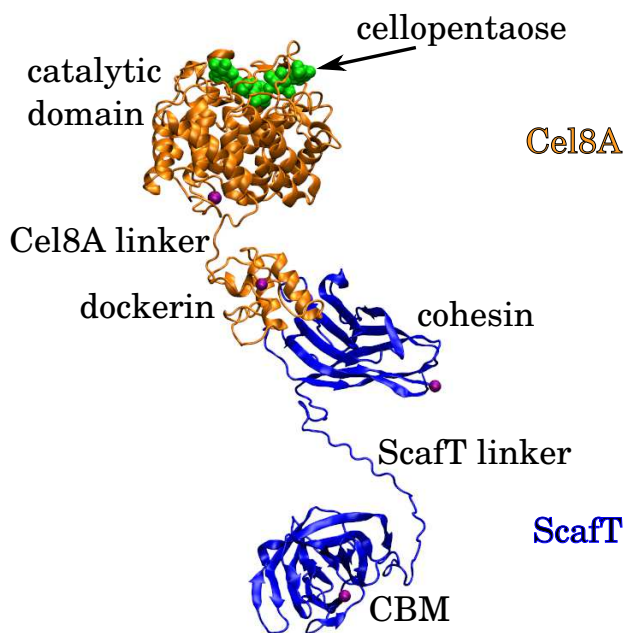


Fig. 1 Structure of the full-length Cel8A-ScaFT complex. Cel8A and ScaFT proteins are shown in orange and blue, respectively. The substrate molecule (cellopentaose) is shown in green. The terminal residues of Cel8A and ScaFT are marked as purple spheres. The functional domains and disordered linkers are indicated. The sequential lengths of the Cel8A and ScaFT linkers are 17 and 25, respectively.

based approaches have been combined to engineer mutants of endoglucanase Cel8A that are thermally more stable and catalytically more active at elevated temperatures than the wild-type Cel8A^{11,12}. In particular, a quadruple mutant has been shown to exhibit a 14-fold increase in the half-life of activity at 85°C¹². This mutant, herein referred to as Cel8A*, contains the following four mutations within its CD as compared to the wild-type protein: K276R, G283P, S329G, S375T. Interestingly, despite the enhanced activity and thermostability of Cel8A* as a free enzyme, its substitution for the wild-type endoglucanase Cel8A within the cellulosome context deteriorates overall degradation of cellulose¹³. For example, the wild-type endoglucanase Cel8A in complex with scaffoldin ScaFT has been demonstrated to exhibit a higher enzymatic activity than the Cel8A*-ScaFT designer cellulosome¹³. These discoveries show that physical interactions between different cellulosomal units can affect the overall enzymatic activity of cellulosomes in a non-trivial way. Here, we investigate what kinds of inter-domain interactions can affect the structure and activity of the Cel8A-ScaFT mini-cellulosome, which is depicted in Fig. 1. Our results indicate that linker-mediated interactions can influence the structure of the active site in Cel8A. We identify differences in the geometry of the substrate-binding region between Cel8A and Cel8A*. We also show that the effective stiffness of the C-terminal linker influences the structure of this region in Cel8A* in a way which is different than in Cel8A.

2 Results

Endoglucanase Cel8A is a glycoside hydrolase of family 8. We consider the endoglucanase Cel8A from *C. thermocellum*, which comprises its CD and a type I dockerin at the C-terminus. Cel8A is shown in orange in Fig. 1. The CD binds to cellulose chains and cleaves their (1 → 4)-β-D-glucosidic linkages. The function of the dockerin domain is to bind tightly to a complementary cohesin domain and, thus, anchor Cel8A to a cellulosomal scaffoldin subunit. The linker between the CD and the dockerin is a proline-rich peptide segment. ScaFT is a section of the *C. thermocellum* cellulosomal CipA scaffoldin subunit¹³. It is shown in blue in Fig. 1. ScaFT contains the family 3a CBM and a single cohesin domain of type I, namely, cohesin 3. The linker between the CBM and the cohesin contains multiple proline and threonine residues. The cohesin binds tightly and specifically to the Cel8A dockerin domain. The function of the CBM is to bind to cellulose chains and, thus, bring the cellulosome to the vicinity of its substrate.

In subsection 2.1 we consider the Cel8A-ScaFT complex in a free state, *i.e.*, when neither the CD nor the CBM are bound to cellulose chains. We next consider a bound state, in which both the CD and the CBM are anchored to cellulose chains. Interestingly, the two 'anchors' impose restraints on the motions of the Cel8A-ScaFT complex. In subsections 2.2 and 2.3 we study the effect of these restraints on the conformations of the CD in Cel8A and Cel8A*, respectively. We find that an important factor is the effective stiffness of the linker between the CD and the remaining parts of the mini-cellulosome in the bound state. In subsection 2.4 we estimate the degree of stiffness of cellulosomal linkers.

2.1 Inter-domain contacts in Cel8A-ScaFT

To examine the physical interactions between the different domains within the free Cel8A-ScaFT complex, we use a coarse-grained model introduced by Kim and Hummer¹⁴. In this model, folded protein domains are treated as rigid bodies and the disordered linkers are simulated as chains of amino-acid beads. This model has been successfully applied to various multi-domain enzymes, including xylanases¹⁵, protein kinases¹⁶ and kinases in dynamic complexes with phosphatases^{17,18}. It involves statistical contact potentials and its description is given in Methods section 3.1. Within the framework of this coarse-grained model, we performed Replica Exchange Monte Carlo simulations of both the wild-type Cel8A-ScaFT complex and the quadruple mutant Cel8A*-ScaFT mini-cellulosome. In these simulations we assumed that the four mutations had only a local effect on the structure of the catalytic domain of Cel8A*. Specifically, our assumption here is that the structures of the catalytic domains of Cel8A and Cel8A* differ only in the chemical composition and orientations of the side chains – and, thus, in the energy of the inter-domain contacts – while the structures of the backbone chains of Cel8A and Cel8A* are identical. Such assumptions are often made in theoretical and computational studies on the effects of mutations on protein stability¹⁹ but do not have to be correct in general.

The simulation results are presented in Supplementary Information. They show that the distributions of the maximum extension for the wild-type Cel8A-ScaFT complex and the quadruple

mutant Cel8A*-ScafT mini-cellulosome are practically identical (see Fig. S1A). Also, there are practically no differences in the distributions of the radius of gyration between Cel8A-ScafT and Cel8A*-ScafT (see Fig. S1B). Moreover, we do not find any systematic differences neither in the probabilities of the inter-domain contacts (see Tab. SI) nor in the end-to-end distance distributions for the flexible linkers (see Fig. S1C and D). In summary, the conformational ensembles of Cel8A-ScafT and Cel8A*-ScafT are found to be practically indistinguishable in these simulations.

Out of the four mutated residues in Cel8A*, two are embedded in the helical core of the CD (G283P and S375T) and two are in loops on the protein surface (K276R and S329G), as indicated in Fig. 2. Moreover, two of the four mutations (K276R and S375T) do not alter the general physicochemical properties of the original residues. Therefore, it is not unreasonable that the four mutations in the catalytic domain do not affect the inter-domain contacts within the Cel8A-ScafT complex. On the other hand, it has been demonstrated that Cel8A-ScafT is more active than Cel8A*-ScafT despite the fact that Cel8A* is more active than Cel8A¹³. Therefore, the interactions between Cel8A and ScafT are relevant for the catalytic activity of the enzyme. These interactions can be direct inter-domain contacts, as investigated here within the framework of the Kim-Hummer model, or indirect linker-mediated interactions.

2.2 Intra-domain contacts within the catalytic domain of Cel8A

2.2.1 Results of coarse-grained structure-based simulations

The Kim-Hummer model does not take into account any structural rearrangements of the individual domains which may be caused by direct domain-domain interactions or by linker-mediated interactions within the protein complex. To study the latter effect, we use a different coarse-grained model, which is structure-based^{23–26} and which is described in detail in Methods section 3.2.

The atomic structure of the catalytic domain of Cel8A in complex with a cellopentaose molecule has been solved²⁷ and deposited in the Protein Data Bank (PDB code 1KWF). It is depicted in Fig. 2. Using the overlap criterion²⁸, we determine both the amino-acid contacts and the contacts between the glucose units and the amino acids within this atomic structure. The overlap criterion predicts 1112 contacts between the amino-acid residues and 30 contacts between the enzyme and its substrate. In the framework of the structure-based coarse-grained model which we use in this study, both the amino-acid residues and the glucose units are represented as single beads that are centered at the α -C and C4 atoms, respectively. All of the native contacts are described by the Lennard-Jones potential acting between the residue beads. Details are given in Methods section 3.2.

The cellopentaose consists of five glucose units which are denoted by S_{-3} , S_{-2} , S_{-1} , S_{+1} and S_{+2} as indicated in Fig. 2. The cellopentaose-binding site in the CD of Cel8A is in the shape of a cleft. The catalytically active residues have the sequence numbers 95 and 152. They are located at the center of the active-site cleft and form contacts with the glucose units S_{-1} and S_{+1} . Unit S_{-3}

connects the cellopentaose to a cellulose chain. To mimic this connection in our model, a virtual spring is attached to the bead representing the glucose unit S_{-3} , see Fig. 2. The Cel8A-ScafT complex binds to cellulose chains also at a different spot *via* its CBM domain. To mimic the linker between the CD and the remaining part of the cellulose-bound Cel8A-ScafT complex, another virtual spring is used. Specifically, it is attached to the LEU395 residue bead at the C-terminus of the CD. These two springs restrain the thermal motion of the CD. The stiffness of the first spring (applied to unit S_{-3}) is set to $\kappa_0 = 160$ kcal/(mol \AA^2), which is equal the stiffness of the pseudo-bond between consecutive beads in our Go-type model. This parameter, denoted by κ_0 , is fixed in all of the simulations we report here. The stiffness of the second spring (applied to LEU395) is denoted by κ . It depends in general on the amino-acid sequence and length of the disordered linkers. It is a variable of our model.

We performed Molecular Dynamics (MD) simulations of the system described above for several different values of the spring constant κ between 0 and 8 kcal/(mol \AA^2). This range of values should capture the persistence lengths of disordered linkers with diverse sequences, as we argue in section 2.4 below. In order to accommodate this wide range, we use a logarithmic scale for κ in the figures.

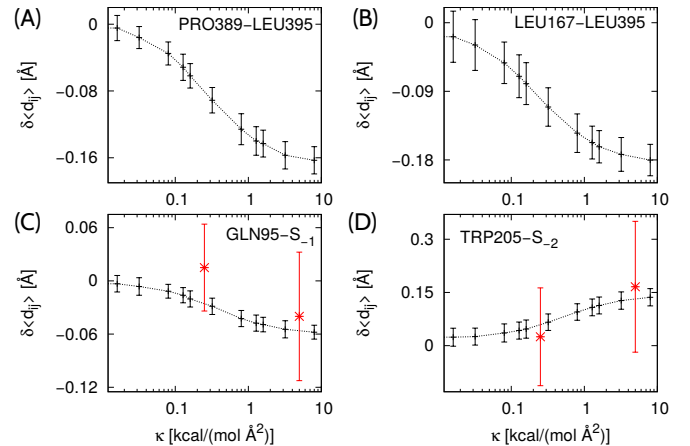


Fig. 3 Variations in the average distance between residues forming native contacts, $\delta\langle d_{ij} \rangle = \langle d_{ij} \rangle(\kappa = 0) - \langle d_{ij} \rangle(\kappa > 0)$, as a function of the stiffness κ of the linker-imitating spring. The residue pairs forming the native contacts are indicated. These residues are indicated by arrows in Fig. 2. Panels A and B refer to two contacts with the C-terminal residue (LEU395). Panels C and D correspond to two contacts within the catalytic cleft. The error bars indicate variations between results from nine independent trajectories. The data points in red correspond to the results of the 30 ns all-atom MD simulations. Note that the logarithmic scale is used on the horizontal axes.

Interestingly, the stiffness of the spring attached to the C-terminus, κ , is observed to have a non-local effect on the average distances $\langle d_{ij} \rangle$ between the residues forming the native contacts. Examples are shown in Fig. 3. Panel A shows how the average distance between PRO389 and LEU395 varies with κ . The latter residue is at the C-terminus, where the second spring is applied. Panel B refers to the contact between LEU167 and LEU395. Panel C corresponds to the contact between the catalytically ac-

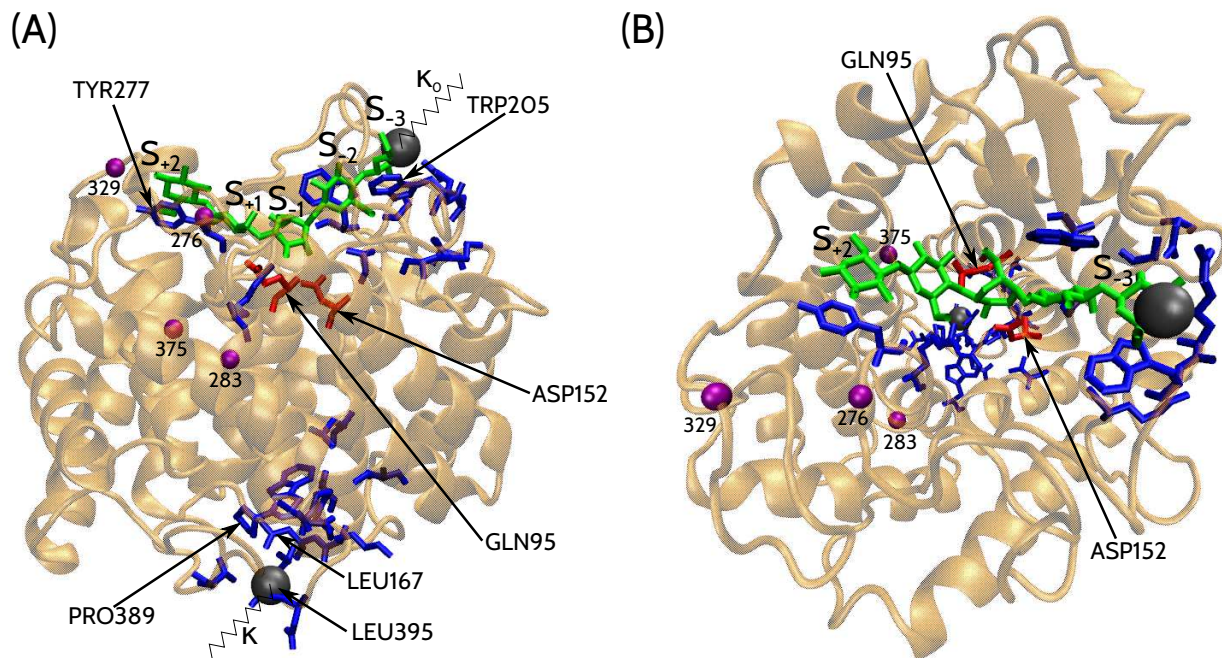


Fig. 2 Structure of the catalytic domain in complex with its substrate. (A) Side view. The gray spheres mark the centers to which the virtual springs are attached: the first one to atom C4 of the glucose ring S_{-3} (upper sphere) and the second one to the α -C atom of LEU395 (lower sphere), which is the C-terminal residue of this domain structure. The corresponding spring constants are denoted by κ_0 and κ . The blue sticks mark the amino-acid residues forming the native contacts that are predicted by the coarse-grained simulations to shorten when the spring is applied to the C-terminal residue. The residues indicated by arrows correspond to the data shown in Fig. 3. The red sticks mark the catalytically active residues with the sequence numbers 95 and 152. The green sticks mark the substrate. The glucose units are labeled by S_{-3} , S_{-2} , S_{-1} , S_{+1} and S_{+2} as in Ref.²⁷. The chemical reaction catalyzed by the endoglucanase results in breaking the bond between S_{-1} and S_{+1} . Unit S_{-3} connects the substrate to a cellulose chain. The purple spheres mark the mutation sites with the sequence numbers 276, 283, 329 and 375 as indicated by the labels. (B) Top view. The color code is the same as in panel A.

tive residue and the glucose unit S_{-1} , where the hydrolysis reaction takes place. In all cases A, B and C, $\langle d_{ij} \rangle$ decreases with increasing κ . In contrast, panel D shows that the average distance between TRP205 and S_{-2} increases with κ . For κ in the range between 0 and 8 kcal/(mol \AA^2), which we have studied here, the changes in the average distance, $\delta \langle d_{ij} \rangle$, are of the order of 0.1 \AA . These distance changes are clearly larger than the statistical errors of $\langle d_{ij} \rangle$, which we have estimated based on nine independent MD trajectories.

In the limiting case of $\kappa = 0$, *i.e.*, when the linker-imitating spring is not applied to the CD, $\langle d_{ij} \rangle$ are observed to have the same values – within the statistical error – as in the case of a free CD with $\kappa = 0$ and $\kappa_0 = 0$, *i.e.*, when no springs are applied to the CD. This result can be seen in the inset of Fig. 4A, where $\Delta_{ij}(\kappa) = \langle d_{ij} \rangle(\kappa) - \langle d_{ij} \rangle_{\text{free}}$ whereas $\langle d_{ij} \rangle_{\text{free}}$ denote the average distances between residue pairs in the free CD. For $\kappa > 0$, most of the native contacts are also practically unaffected by the attachment of the two springs. However, there is a group of about five native contacts that are observed to become longer as a result of applying the linker-imitating spring. They are marked in Fig. 4A in green. There is also a group of over twenty native contacts that become distinctly shorter upon applying this spring. These contacts are marked in red in Fig. 4A. The amino acids that form these contacts are shown as blue sticks in Fig. 2. It is interesting to note that the contact-length changes are observed

to occur in many residue pairs in the vicinity of the substrate. This observation implies that variations in κ lead to changes in the geometry of the substrate-binding region. We predict these geometrical changes to be rather small because $\delta \langle d_{ij} \rangle$ are of the order of 0.1 \AA only. However, in general, the catalytic activity of enzymes requires very precise positioning of substrate molecules in the active site. We therefore suggest that the linker-induced, small structural rearrangements of the active site cleft may influence the activity of Cel8A.

We also performed MD simulations of the CD without the substrate molecule in the catalytic cleft. The PDB structure 1CEM was used as input for these simulations, and only one spring was attached to the CD, *i.e.*, the one at the C-terminus with the effective stiffness κ . We find that regardless of the value of κ , the average distances $\langle d_{ij} \rangle$ are practically the same as in the case of the free catalytic domain that is not attached to any spring. These simulation results show that the linker-induced changes in the active site conformations can occur only in the bound state. We note that these conformational changes result from the restrains that are imposed on the mini-cellulosome by its attachment to cellulose chains at two distinct sites.

We also analyzed root-mean-square fluctuations of individual residues, δ_i , as defined by Eq. (7). The fluctuations of the great majority of residues are essentially unaffected by the stiffness of the second spring. Several exceptions are shown in Fig. 4B. We

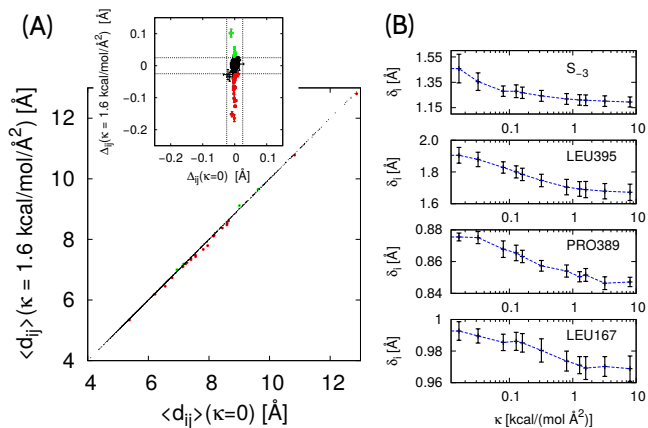


Fig. 4 Results of the coarse-grained structure-based MD simulations. (A) $\langle d_{ij} \rangle$ computed for $\kappa = 0$, i.e., when only one spring with stiffness κ_0 is attached to residue S_{-3} , versus $\langle d_{ij} \rangle$ for $\kappa = 1.6$ kcal/mol/Å². The elongated contacts are marked in red. The shortened contacts are marked in green. Inset: $\Delta_{ij}(\kappa = 0)$ versus $\Delta_{ij}(\kappa = 1.6$ kcal/mol/Å²), where $\Delta_{ij}(\kappa) = \langle d_{ij} \rangle(\kappa) - \langle d_{ij} \rangle_{\text{free}}$ and $\langle d_{ij} \rangle_{\text{free}}$ denotes the average inter-residue distances in a free CD which is not attached to any spring. (B) Root-mean-square fluctuations δ_i of the indicated residues as a function of the spring constant κ . These residues are depicted in Fig. 2.

note that the influence of the linker-imitating spring on δ_i is local – only the spring attachment sites (LEU395 and S_{-3}) and its nearest neighbors exhibit a dependence of δ_i on κ . Specifically, δ_i decreases with increasing κ for these residues.

As mentioned before, the structural changes in Cel8A are relatively small (variations in $\langle d_{ij} \rangle$ do not exceed 0.2 Å; variations in δ_i are below 0.3 Å) but very non-local (they propagate throughout the entire enzymatic domain). These small structural changes should be captured correctly by the structure-based model because its predictions are expected to be most accurate in a vicinity of the native state.

2.2.2 Results of all-atom MD simulations

To validate the results of the coarse-grained MD simulations, we performed several all-atom MD simulations with explicit water, as described in Methods section 3.3. We used NAMD version 2.9 with CHARMM force fields and TIP3P water model. As in the coarse-grained simulations, one spring was attached to atom C4 of the glucose unit S_{-3} , and another one to the α -C atom of the amino-acid residue LEU395.

To start, we performed four independent, short simulations, 2 ns each, in which the virtual spring attached to the C-terminus had the stiffness κ of 0, 0.05, 0.5 and 5 kcal/(mol Å²), respectively. The simulation structures were recorded every 1 ps, which resulted in generating 2000 ‘frames’ for each of the four values of κ . Any ‘frame’ represented a simulation structure at a given time instant between 0 and 2 ns. Next, each of the frames was analyzed individually by an external program to determine the instantaneous contacts between the enzyme and its substrate. The contacts were identified using the overlap criterion. It turns out that some of the protein-sugar contacts persist throughout all of the frames. However, most of the contacts exist only in a fraction of the recorded frames. We denote this fraction by f_{ij} , where

the subscript ij labels the residues forming the contact. Fig. 5A shows the number of contacts between Cel8A and its substrate, n_c , as a function of f_{ij} for $\kappa = 0, 0.05, 0.5$ and 5 kcal/(mol Å²). For a given fraction f_{ij} , n_c generally increases with κ , especially for the most stable contacts with $f_{ij} > 0.95$. This result indicates that the stiffness of the linker-imitating spring affects the interactions between Cel8A and its substrate on the time scale of a few nanoseconds. Generally, increasing κ leads to an increased stability of instantaneous contacts.

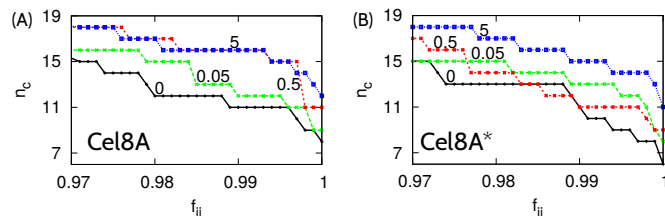


Fig. 5 The number of residue contacts between the endoglucanase and the cellopentaose, n_c , which are present in a given fraction f_{ij} of the recorded frames. These results correspond to the short, 2 ns, all-atom MD simulation trajectories. The labels 0, 0.05, 0.5 and 5 indicate the stiffness of the C-terminal spring, κ , given in the units of kcal/(mol Å²), which correspond to the black, green, red and blue lines, respectively. Panels A and B correspond to the wild type (Cel8A) and mutant (Cel8A*) enzyme, respectively.

We also generated three longer trajectories, 30 ns each, in which the stiffness of the linker-imitating spring, κ , was taken to have the following values: 0 (meaning no spring attached to LEU395), 0.25 kcal/(mol Å²) (soft spring) and 5 kcal/(mol Å²) (stiff spring). Based on these longer trajectories, we computed the average distances between the α -C and C4 atoms in the residues forming the native contacts between Cel8A and its substrate. Our goal was to directly compare these distances with the contact-length changes that we observed in the coarse-grained simulations. Examples of such a comparison are shown in Fig. 3C and D, which correspond to the native contacts GLN95- S_{-1} and TRP205- S_{-2} , respectively. The results of the all-atom and coarse-grained simulations seem to be consistent. However, the statistical errors on $\langle d_{ij} \rangle$ from all-atom simulations are larger than the effect of contact-length changes. The significant statistical errors reflect most likely insufficient sampling in the all-atom simulations. In fact, the time scales of the all-atom (30 ns) and coarse-grained (0.5 ms) simulations are incomparable. Nevertheless, the all-atom MD simulations turn out to be very useful for studies on the effect of mutations in Cel8A, which we will discuss in the next section.

2.3 Intra-domain contacts within the catalytic domain of Cel8A*

We use FoldX¹⁹ to generate an atomic structure of the CD of the four-point mutant Cel8A*. In this approach, the four mutations (K276R, G283P, S329G, S375T) are assumed to have only a local effect on the structure of the CD. Specifically, the structures of the backbone chains of Cel8A and Cel8A* are assumed to be identical.

2.3.1 Results of coarse-grained structure-based simulations

Using the overlap criterion²⁸ we determine native contacts within the mutant structure. The overlap criterion predicts 1117 contacts between amino acids and 30 contacts between the enzyme and its substrate. The four mutations introduce nine new contacts and cause four contacts to vanish. However, they do not change the native contacts between the protein and the substrate.

To study the equilibrium properties of the mutant enzyme (Cel8A* CD) in the vicinity of its native state, we used the same coarse-grained structure-based model as for the simulations of the wild-type enzyme (Cel8A CD). Two virtual spring were attached to Cel8A* CD in complex with cellopentaose: the first one to unit S₋₃ of the substrate molecule and the second one to the C-terminal residue (LEU395). The attachment sites for the springs were thus the same as those in Cel8A CD.

We performed coarse-grained MD simulations of this system for several different values of κ ranging from 0 to 8 kcal/(mol Å²). We analyzed the average distances between the residue pairs forming native contacts, $\langle d_{ij} \rangle$, and found that the great majority of them were unaffected by the four mutations. However, we notice several exceptions, two of which are depicted in Fig. 6. The blue and red lines correspond to Cel8A and Cel8A*, respectively. Panel A shows $\langle d_{ij} \rangle$ as a function of κ for the native contact between residue TYR277 and the glucose unit S₊₁. Panel B corresponds to $\langle d_{ij} \rangle(\kappa)$ for the residue pair TRP205 and TRP260. The former amino-acid residue participates in the binding of the cellopentaose in the catalytic cleft. In both cases A and B, systematic differences in $\langle d_{ij} \rangle(\kappa)$ are observed between Cel8A CD and Cel8A* CD. In contrast, panels C and D – which correspond to the same residue pairs as panels C and D in Fig. 3 – show two examples where $\langle d_{ij} \rangle(\kappa)$ are practically identical for Cel8A CD and Cel8A* CD. These results indicate that the stiffness of the linker-imitating spring can affect the geometry of the catalytic cleft region in Cel8A and Cel8A* in different ways.

The contacts between the enzyme and its substrate are the same in Cel8A* CD and Cel8A CD. However, the average lengths of several of these contacts are different. Namely, the contact between TYR277 and S₊₁ is found to shorten upon introducing the mutations, as shown in Fig. 6A. There are also three contacts that are observed to become slightly longer as a result of the mutations: ARG84-S₊₁, ARG84-S₋₁ and ALA150-S₋₁. As shown in Fig. 6E, TYR277 and ARG84 are located on the opposite sides of the catalytic cleft. Therefore, the coarse-grained simulations indicate that the four mutations lead to a small shift of units S₊₁ and S₋₁ from one side of the catalytic cleft to another. We note, however, that our assumption about identical structures of the backbone chains of Cel8A and Cel8A* may not be correct. In fact, the four mutations may lead to non-local changes in the CD structure. In such cases, there would be more differences in the contact maps for Cel8A and Cel8A*. We would then expect the differences in $\langle d_{ij} \rangle(\kappa)$ between Cel8A and Cel8A* to be even more evident.

2.3.2 Results of all-atom MD simulations

To test the predictions of the coarse-grained model, we performed all-atom MD simulations with explicit water as described in Meth-

ods section 3.3. We performed four short simulations, 2 ns each, and analyzed the instantaneous contacts using the same method as in the case of Cel8A simulations. Fig. 5B shows the number of contacts between Cel8A* and its substrate, n_c , which are observed in a given fraction f_{ij} of the recorded frames. The black, green, red and blue lines correspond to $\kappa=0, 0.05, 0.5$ and 5 kcal/(mol Å²), respectively. As in the case of the wild type enzyme, n_c as a function of f_{ij} generally increases with increasing κ . This result indicates that increasing the stiffness of the linker-imitating spring leads to an increased stability of the instantaneous contacts on the time scales of a few nanoseconds.

As discussed in the previous subsection, the coarse-grained simulations predict that four contacts between the enzyme and its substrate change their lengths when Cel8A is mutated to Cel8A*: TYR277-S₊₁, ARG84-S₊₁, ARG84-S₋₁, and ALA150-S₋₁. We performed 30 ns all-atom MD simulations of Cel8A CD and Cel8A* CD, with $\kappa=0, 0.25$ and 5 kcal/(mol Å²), and measured the average distances between the α -C and C4 atoms in these four pairs of residues. We found that the average distances were indeed different in Cel8A and Cel8A*, as shown in Fig. 7. Both the coarse-grained and all-atom simulations show that TYR277-S₊₁ shortens upon introducing the mutations. However, the magnitude of the length changes is larger in the all-atom simulations, see Fig. 6A and the blue data points in Fig. 7A. Moreover, the coarse-grained simulations predict that ARG84-S₊₁ and ARG84-S₋₁ become slightly longer as a result of the mutations, which suggests a small shift of units S₊₁ and S₋₁ from one side of the catalytic cleft to another. This prediction is inconsistent with the results of the all-atom simulations, in which ARG84-S₊₁ and ARG84-S₋₁ become significantly shorter, by about about 2 Å, upon introducing the mutations into the catalytic domain. Visual inspection of the all-atom trajectories reveals that the rings S₋₁, S₊₁ and S₊₂ are embedded somewhat deeper in the catalytic cleft of Cel8A* in comparison to the location of the cellopentaose molecule in the catalytic cleft of Cel8A.

The all-atom simulations show that there are many contacts between the enzyme and its substrate which – within the simulation error – do not change their lengths when Cel8A is mutated to Cel8A*. Three examples are shown in Fig. 7B, where the black and red data points correspond to GLN95-S₋₁ and TRP215-S₋₂, respectively. These two contacts were found to be unaffected by the mutations also in the coarse-grained simulations. In contrast, the contact between ALA150 and S₋₁ seems to be unchanged in the all-atom simulations (blue data points in Fig. 7B) but it is found to elongate by about 0.02 Å in the coarse-grained simulations. However, such small changes in the contact length can not be identified in the all-atom simulations due to the statistical errors and insufficient sampling.

Despite the fact that the coarse-grained and all-atom simulations give consistent predictions about the length changes of certain native contacts, they do not agree qualitatively in general. The major reason for this disagreement is most likely the assumption underlying the coarse-grained model that the backbone chains of Cel8A and Cel8A* are identical. Nevertheless, both the coarse-grained simulations and the all-atom simulations show that the four mutations in the endoglucanase as well as

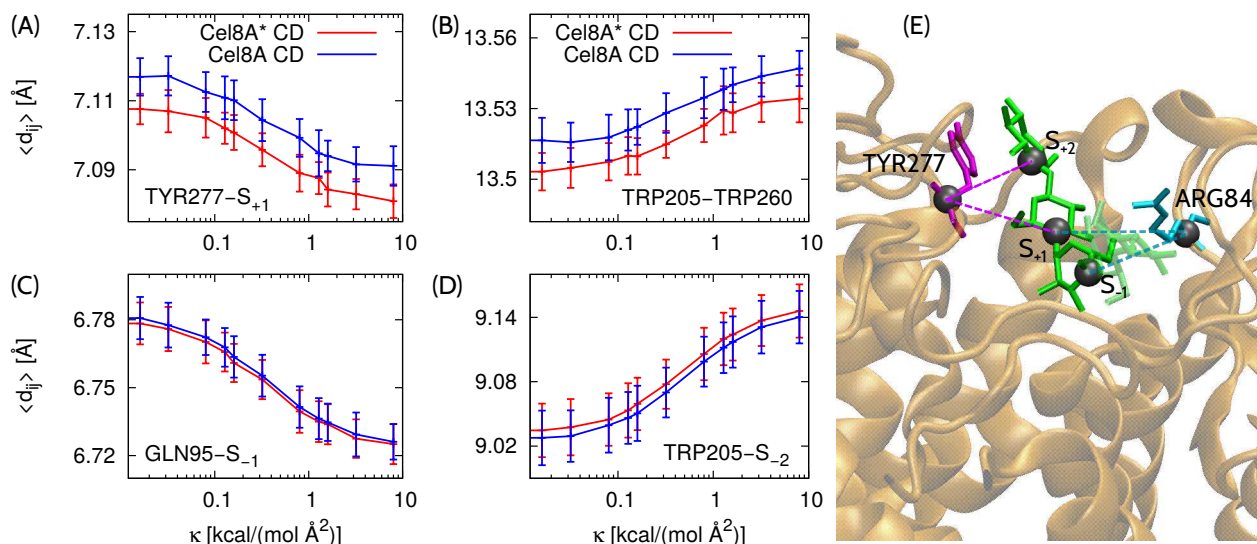


Fig. 6 (A-D) $\langle d_{ij} \rangle$ as a function of κ for indicated residue pairs within the CD of Cel8A (blue lines) and Cel8A* (red lines). These distances were determined in the coarse-grained MD simulations. Note that the logarithmic scale is used on the horizontal axes. (A) Simulation results corresponding to the contact between TYR277 and the sugar unit S₊₁. This contact is marked as a dashed line in panel E. (B) Simulation data corresponding to the amino-acid contact between TRP205 and TRP260. The former residue participates in binding of the cellopentaose in the catalytic cleft. (C and D) The same residue pairs as in panels C and D of Fig. 3. These contacts are predicted by the coarse-grained MD simulations to be unaffected by the mutations. (E) Geometry of the catalytic cleft. Cellopentaose is shown in green, TYR277 in purple, and ARG84 in cyan. The gray spheres mark the α -C atoms of the two amino acids and the C4 atoms of the sugar units S₋₁, S₊₁ and S₊₂.

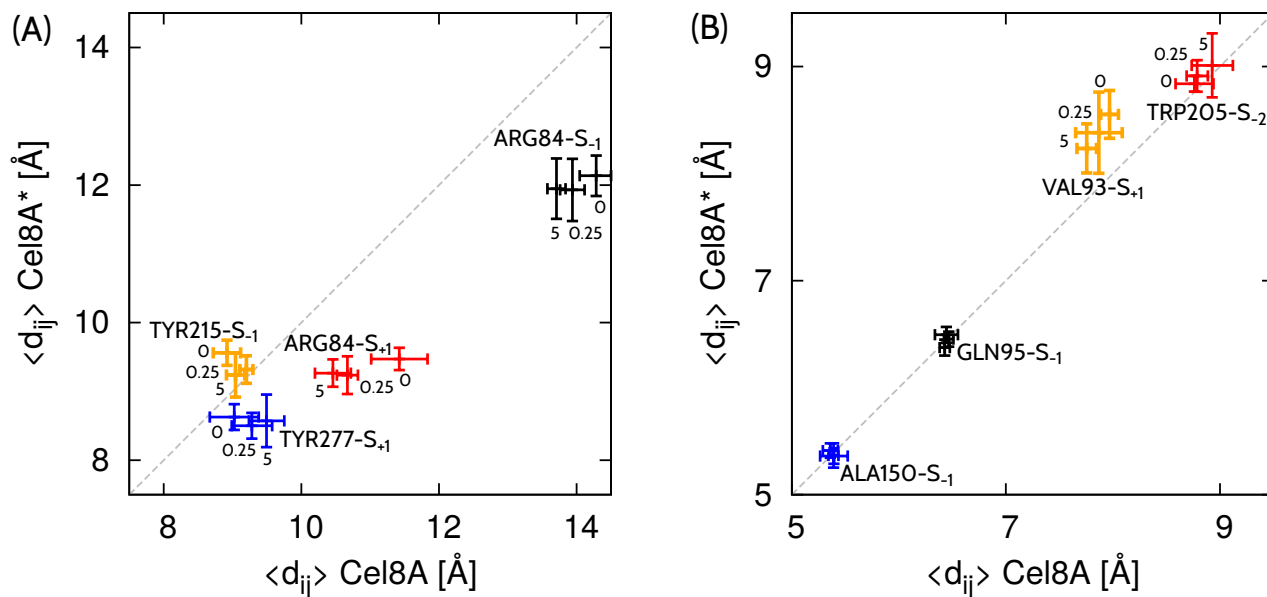


Fig. 7 $\langle d_{ij} \rangle$ in Cel8A versus $\langle d_{ij} \rangle$ in Cel8A* for indicated contacts between the endoglucanase and the cellopentaose molecule. These distances were measured in the 30 ns MD simulations. The labels 0, 0.25 and 5 indicate the values of κ given in the units of kcal/(mol Å²). (A) Four contacts for which $\langle d_{ij} \rangle(\kappa)$ in Cel8A and Cel8A* are clearly different. Three of the indicated contacts (TYR277-S₊₁, ARG84-S₊₁ and ARG84-S₋₁, see Fig. 6D) have been predicted by the coarse-grained simulations to have different lengths in Cel8A and Cel8A*. For example, the blue data points indicate the contact between TYR277 and S₊₁, which corresponds to Fig. 6A. (B) Four contacts for which $\langle d_{ij} \rangle(\kappa)$ are practically unaffected, or affected only weakly (VAL93-S₊₁), by the mutations in the endoglucanase. The black and red data points indicate GLN95-S₋₁ and TRP215-S₋₂, respectively, which correspond to Fig. 6C and D.

variations in the stiffness of the linker-mimicking spring, κ , lead to noticeable changes in the average lengths of certain contacts between the enzyme and its substrate. Moreover, the contact-length changes due to variations in κ can be different in Cel8A and Cel8A*, see Figs. 6 and 7.

2.4 Estimates on the stiffness of disordered linkers

In our recent work on conformational variability of the multi-domain xylanase Z (XynZ) of *C. thermocellum*, we determined the average end-to-end distance, $\langle d_{ee} \rangle$, and the root-mean-square end-to-end distance, $\langle d_{ee}^2 \rangle^{1/2}$ for the three disordered linkers of the sequential length of 6, 12 and 24 amino-acid residues¹⁵. From the variance of the end-to-end distance, $\langle d_{ee}^2 \rangle - \langle d_{ee} \rangle^2$, we can estimate the effective spring constant, κ , which corresponds to such distance variations as induced by thermal fluctuations. In fact, equipartition of energy implies that

$$\frac{1}{2} \kappa (\langle d_{ee}^2 \rangle - \langle d_{ee} \rangle^2) = \frac{3}{2} k_B T \quad (1)$$

and thus

$$\kappa = \frac{3k_B T}{\langle d_{ee}^2 \rangle - \langle d_{ee} \rangle^2} \quad (2)$$

At room temperature, $T = 300$ K, we obtain $\kappa = 0.26$ kcal/(mol Å²), $\kappa = 0.07$ kcal/(mol Å²) and $\kappa = 0.02$ kcal/(mol Å²) for the three linkers that are formed of 6, 12 and 24 amino-acid residues, respectively. Note that κ exhibits a 14-fold decrease when the sequential length of the linkers increases from 6 to 24. It is because of this effect that we use the logarithmic scale in Figs. 3 and 6.

These values of κ are obtained for the three linkers within XynZ that have a specific amino-acid sequence. In general, $\langle d_{ee}^2 \rangle - \langle d_{ee} \rangle^2$ should depend not only on the sequential length of the linkers but also on their composition. Therefore, amino-acid mutations within linkers can lead to changes in the effective stiffness κ .

3 Methods

In this work we have employed three types of simulations: (i) coarse-grained Monte Carlo simulations that are used to characterize the conformational ensemble of the full-length Cel8A-ScaFT complex; (ii) coarse-grained, structure-based Molecular Dynamics simulations that are used to investigate the influence of the linker-mimicking spring on the structure of the catalytic domain of Cel8A and Cel8A*; and (iii) all-atom Molecular Dynamics simulations that give insights into the effect of the four-point mutation on the enzyme-substrate interactions. These simulation methods will be described in the following three subsections.

3.1 Coarse-grained simulations of Cel8A-ScaFT and Cel8A*-ScaFT

To sample physical conformations of the full-length Cel8A-ScaFT complex, we use a coarse-grained model equipped with a transferable energy function that has been developed to simulate protein binding¹⁴. In the framework of this model, amino acid residues are represented as spherical beads centered at the α -C atoms. The interactions between the residue beads are de-

scribed by short-range Lennard-Jones (LJ) type potentials and long-range electrostatic potentials. The electrostatic interactions are described by a Debye-Hückel-type potential. The LJ-type potentials are characterized by (i) amino-acid dependent interaction strengths, $\tilde{\epsilon}_{ij}$, which are adapted from knowledge-based statistical contact potentials introduced by Miyazawa and Jernigan²⁰, and (ii) residue-dependent interaction radii $\tilde{\sigma}_{ij} = (\tilde{\sigma}_i + \tilde{\sigma}_j)/2$, where $\tilde{\sigma}_i$ is the van der Waals diameter of residue i , which is calculated from the van der Waals volume by assuming a spherical shape for the residue, see Table 5 in Ref. ¹⁴.

Folded protein domains are represented as rigid bodies whereas flexible linker peptides connecting the domains are represented as polymers of amino acid beads with bending, stretching and torsion potentials. A detailed description of the model can be found in Ref. ¹⁴. The full-length model of the Cel8A-ScaFT complex comprises three rigid domains: (i) the catalytic domain of endoglucanase Cel8A (PDB code 1CEM), (ii) the carbohydrate-binding module of family 3a (CBM3A with the PDB code 4JO5), and (iii) the dockerin domain of the endoglucanase Cel8A in complex with the cohesin-3 domain of the scaffoldin CipA. To the best of our knowledge, there is no PDB entry with the structure of the dockerin-cohesin complex that corresponds to the rigid body (iii). For this reason we use a homology model generated by SWISS-MODEL²¹ with the PDB structures 1AOH and 4DH2 as templates for the cohesin (94 percent sequence identity) and dockerin (43 percent sequence identity), respectively. In this homology model, the dockerin-cohesin interface is analogous to that found in the PDB structure 4DH2. In addition to the three rigid bodies, the full-length model of Cel8A-ScaFT comprises two flexible linkers, as shown in Fig. 1. The sequential length of the Cel8A and ScaFT linkers is 17 and 25 amino acids, respectively. Their amino acid sequences are given in Supplementary Information. We generated the initial configurations of the disordered linkers using Mod-Loop²².

We performed Replica Exchange Monte Carlo (REMC) simulations using in-house software with replicas at sixteen different temperatures T_i given by $T/T_i = 0.6, 0.64, \dots, 1.16, 1.2$ relative to the room temperature $T = 300$ K. The basic MC steps were rigid body translational and rotational moves on each domain. For flexible linker peptides, in addition to local MC moves on each residue, crank shaft moves were employed to enhance sampling. The probabilities of the MC moves were governed by the Metropolis criterion. After the initial 10^6 MC sweeps for equilibration, 10^7 MC sweeps were performed for data acquisition. The protein conformations were saved every 10^3 MC sweeps, which gave us an ensemble of 10^4 conformations for further analysis. In order to check that the simulation results were not biased by the initial conformation, we performed five independent simulation runs that were started with different seeds for the random number generator.

3.2 Coarse-grained simulations of the catalytic domain

To sample near-native conformations of the catalytic domain of endoglucanase Cel8A in complex with its substrate (cellopentaose), we use our coarse-grained structure-based model²³⁻²⁶,

in which amino-acid residues and sugar units are represented by single beads centered on their α -C and C4 atoms, respectively. The beads are tethered together into two chains by strong harmonic potentials with the spring constant of $100\epsilon/\text{\AA}^2$, where ϵ is the depth of the potential well associated with the native contacts, which serves as the basic energy scale in this model. The chain of amino-acid beads corresponds to the enzyme and the chain of glucose-ring beads corresponds to its substrate. The native contacts are identified using an overlap criterion²⁸ applied to the coordinates of all heavy atoms in the native structure (PDB code 1KWF²⁷). The van der Waals radii for the heavy atoms of amino acids and sugar residues are taken from Refs.²⁹ and²⁶, respectively. The amino acid pairs that are very close sequentially, $(i, i+1)$ and $(i, i+2)$, are excluded from the contact map²⁴. The contacts between the protein and the substrate are treated in the same manner as the contacts within the protein as both sets are dominated by hydrogen bonds²⁵.

The interactions within the native contacts are described by the Lennard-Jones potential

$$V^{\text{NAT}}(r_{ij}) = 4\epsilon \left[\left(\frac{\sigma_{ij}}{r_{ij}} \right)^{12} - \left(\frac{\sigma_{ij}}{r_{ij}} \right)^6 \right] \quad (3)$$

Here, r_{ij} is the distance between residue beads i and j forming the native contact, and the parameters σ_{ij} are chosen so that each contact in the native structure is stabilized at the minimum of the Lennard-Jones potential. The value of ϵ is approximately given by (1.6 ± 0.4) kcal/mol, as has been determined by comparing simulational results to the experimental ones on a set of 38 proteins²⁴. The interactions between the pairs of residue beads that do not form native contacts are purely repulsive and given by a truncated and shifted Lennard-Jones type potential

$$V^{\text{NON-NAT}}(r_{ij}) = 4\epsilon \left[\left(\frac{\sigma_0}{r_{ij}} \right)^{12} - \left(\frac{\sigma_0}{r_{ij}} \right)^6 + \frac{1}{4} \right] \quad \text{for } r_{ij} \leq r_0 \quad (4)$$

and $V^{\text{NON-NAT}}(r_{ij}) = 0$ for $r_{ij} > r_0$. Here, $\sigma_0 = r_0/\sqrt[6]{2}$ and $r_0 = 4 \text{ \AA}$. The potential energy comprises also harmonic terms that favor the native values of the local chirality³⁰. Specifically, we use

$$V^{\text{C}} = \frac{k_c}{2} \sum_{i=2}^{N-2} \left(C_i - C_i^{\text{NAT}} \right)^2 \quad \text{with } C_i = \frac{(\vec{w}_{i-1} \times \vec{w}_i) \cdot \vec{w}_{i+1}}{d_i^3} \quad (5)$$

Here, C_i^{NAT} and C_i denote the chirality of residue i in the native and instantaneous conformation, respectively, $\vec{w}_i = \vec{r}_{i+1} - \vec{r}_i$, and $d_i = |\vec{w}_i|$ is the distance between subsequent residue beads i and $i+1$. We take $k_c = \epsilon$, as in Ref.³⁰. By construction, the global minimum of the potential energy corresponds to the native structure.

The solvent is implicit and the system evolves in time according to the Langevin dynamics. The overall force acting on a particular bead i is a sum of three terms: (i) the direct force \vec{F}_i that derives from all the potential terms, (ii) the damping force that is proportional to the velocity of the bead, and (iii) the random force, $\vec{\Gamma}_i$, that represents thermal noise. The corresponding equations of

motion

$$m \frac{d^2 \vec{r}_i}{dt^2} = \vec{F}_i - \gamma \frac{d\vec{r}_i}{dt} + \vec{\Gamma}_i \quad (6)$$

are solved by the fifth order predictor-corrector algorithm with the time step of 0.005τ using in-house software. Here, γ is the damping coefficient and all beads are assumed to have the same mass m . The dispersion of the noise is given by $\sqrt{2\gamma k_B T}$, where k_B is the Boltzmann constant and T denotes the temperature. All of the simulations reported here are performed at $k_B T = 0.3 \epsilon$, which is near-optimal in folding kinetics and is of order of the room temperature. The damping coefficient is set to $\gamma = 2m/\tau$. This value corresponds to the overdamped case – practically Brownian dynamics – and the characteristic time scale, τ , is of the order of 1 ns, as argued in Refs.^{31,32}. The average distances $\langle d_{ij} \rangle$ between pairs of beads (i, j) within native contacts are computed from nine independent trajectories of $6 \times 10^4 \tau$ each. The trajectories start from the native state with different seeds for the random number generator, and the first $10^4 \tau$ are used for equilibration and excluded from computing $\langle d_{ij} \rangle$.

To quantify the local flexibility of the enzyme, we compute the root-mean-square fluctuation (RMSF) of each residue

$$\delta_i = \left[\langle \vec{r}_i^2 \rangle - \langle \vec{r}_i \rangle^2 \right]^{1/2} \quad (7)$$

Here, \vec{r}_i is the position of the i -th residue and the angle brackets denote the average after superimposing on the native structure.

3.3 All-atom simulations of the catalytic domain

The atomic coordinates of the catalytic domain in complex with the cellopentaose were taken from the crystal structure reported in Ref.²⁷ (PDB code 1KWF). The atomic structure of the four-point mutant was generated using FoldX¹⁹. The initial systems for all-atom MD simulations were prepared using VMD³³. Namely, the structures were solvated using Solvate Plugin version 1.5. Sodium and chloride ions were added to neutralize the simulated system and to reach a physiological ion concentration of 150 mM.

The all-atom MD simulations were performed using NAMD 2.9³⁴. CHARMM22 force field³⁵ with CMAP correction³⁶ was used for proteins. The parameters of CHARMM36 force field^{37–39} were employed for the cellopentaose. The TIP3P water model was used⁴⁰. The simulations were carried out in the NPT ensemble. Temperature was kept at 300 K through a Langevin thermostat with a damping coefficient of 1/ps. Pressure was maintained at 1 atm using the Langevin piston Nose-Hoover method with a damping timescale of 50 fs and an oscillation timescale of 100 fs. Short-range non-bonded interactions were cut off smoothly between 10 and 12 \AA . Long-range electrostatic interactions were computed using the particle-mesh Ewald method with a grid spacing of 1 \AA . Simulations were performed with an integration time step of 2 fs.

Prior to the actual simulations, the system was relaxed in three subsequent steps: (i) relocation of atoms and water molecules with 10000 iterations of a conjugate gradient energy minimization; (ii) 0.1 ns simulation at temperature $T = 100$ K; and (iii) 0.1 ns simulation at $T = 200$ K. We performed several short, 2 ns

simulations as well as longer, 30 ns simulations of both the wild type CD and the four-point mutant CD. The stiffness of the virtual spring attached to the α -C atom of the C-terminal residue LEU395 was taken to have several different values in these simulations, as specified in Results sections 2.2.2 and 2.3.2.

4 Summary

Significant efforts have been made to identify and implement mutations that improve stability and activity of individual domains of cellulosomes. However, the recent discoveries made by the Bayer group show that enhancing thermostability and activity of separate enzymatic domains need not necessarily lead to an improvement in overall degradation of cellulose by designer cellulosomes¹³. Our results indicate that mutations that change the effective stiffness of the disordered linkers can modulate the enzyme structure in a non-local manner. These mutations may involve insertions and deletions, which change the linker length, or amino-acid replacements that influence the persistence length of linkers. The resulting modulations of the enzyme structure may in turn imply changes in the activity of cellulosomal enzymes. Our results may thus help explain the reasons for the astonishing variability in sequences among the cellulosomal linkers. Our results may also shed light on the discovery made by the Bayer group that designer cellulosomes assembled with the native long-linker scaffoldins achieve higher levels of activity compared to those assembled with short-linker scaffoldins⁴.

Disordered and flexible linkers are found in various multi-domain proteins^{41,42}. It would be thus interesting to study whether the elastic properties of linkers could influence the activity of other multi-domain enzymes. Interestingly, in several regulatory proteins, linkers have been reported to serve not only as passive tethers but also as active modulators of the function elicited by adjacent domains^{43–45}. In particular, recent experiments on protein kinase C show that inter-domain linkers play critical roles in stabilizing certain conformation⁴⁶.

Acknowledgements

This research has been supported by the European Framework Programme VII NMP grant 604530-2 (CellulosomePlus), the ERA-NET-IB/06/2013 Grant FiberFuel funded by the National Centre for Research and Development in Poland, and the Grant 2014/15/B/ST3/01905 from the National Science Centre. It was also co-financed by the Polish Ministry of Science and Higher Education from the resources granted for the years 2014-2017 in support of international scientific projects.

References

- 1 Y. Shoham, R. Lamed and E.A. Bayer, *The cellulosome concept as an efficient microbial strategy for the degradation of insoluble polysaccharides*, Trends Microbiol., 1999, **7**, 275-281.
- 2 E.A. Bayer, J.P. Belaich, Y. Shoham and R. Lamed, *The cellulosomes: Multi-enzyme machines for degradation of plant cell wall polysaccharides*, Annu. Rev. Microbiol., 2004, **58**, 521-554.
- 3 E.A. Bayer, R. Lamed and M.E. Himmel, *The potential of cellulases and cellulosomes for cellulosic waste management*, Curr. Opinion Biotechnol., 2007, **18**, 237-245.
- 4 Y. Vazana, Y. Barak, T. Unger, Y. Peleg, M. Shamshoum, T. Ben-Yehzekel, Y. Mazar, E. Shapiro, R. Lamed and E.A. Bayer, *A synthetic biology approach for evaluating the functional contribution of designer cellulosome components to deconstruction of cellulosic substrates*, Biotechnol Biofuels., 2013 **6**, 182.
- 5 M. Hammel, H.P. Fierobe, M. Czjzek, V. Kurkal, J.C. Smith, E.A. Bayer, S. Finet and V. Receveur-Brechot, *Structural basis of cellulosome efficiency explored by small angle X-ray scattering*, J. Biol. Chem., 2005, **280**, 38562-38568.
- 6 M. Czjzek, H.P. Fierobe and V. Receveur-Brechot, *Small-angle X-ray scattering and crystallography: A winning combination for exploring the multimodular organization of cellulytic macromolecular complexes*, Methods in Enzymology, 2012, **510**, 183-210.
- 7 M.A. Currie, J.J. Adams, F. Faucher, E.A. Bayer, Z.C. Jia and S.P. Smith, *Scaffoldin conformation and dynamics revealed by a ternary complex from the Clostridium thermocellum cellulosome*, J. Biol. Chem., 2012, **287**, 26953-26961.
- 8 M.A. Currie, K. Cameron, F.M.V. Dias, H.L. Spencer, E.A. Bayer, C.M.G.A. Fontes, S.P. Smith and Z. Jia, *Small angle X-ray scattering analysis of Clostridium thermocellum cellulosome N-terminal complexes reveals a highly dynamic structure*, J. Biol. Chem., 2013, **288**, 7978-7985.
- 9 J. Caspi, Y. Barak, R. Haimovitz, D. Irwin, R. Lamed, D.B. Wilson and E.A. Bayer, *Effect of Linker Length and Dockerin Position on Conversion of a Thermobifida fusca Endoglucanase to the Cellulosomal Mode*, Appl. Environ. Microbiol., 2009, **75**, 7335-7342.
- 10 C.L. Ting, D.E. Makarov and Z.-G. Wang, *A kinetic model for the enzymatic action of Cellulase*, J. Phys. Chem. B, 2009, **113**, 4970-4977.
- 11 M. Anbar, R. Lamed and E.A. Bayer, *Thermostability Enhancement of Clostridium thermocellum Cellulosomal Endoglucanase Cel8A by a Single Glycine Substitution*, ChemCatChem, 2010, **2**, 997-1003.
- 12 M. Anbar, O. Gul, R. Lamed, U.O. Sezerman and E.A. Bayer, *Improved Thermostability of Clostridium thermocellum Endoglucanase Cel8A by Using Consensus-Guided Mutagenesis*, Applied and Environmental Microbiology, 2012, **78**, 3458-3464.
- 13 J. Stern, M. Anbar, S. Morais, R. Lamed and E.A. Bayer, *Insights into enhanced thermostability of a cellulosomal enzyme*, Carbohydrate Research, 2014, **389**, 78-84.
- 14 Y.-C. Kim and G. Hummer, *Coarse-grained models for simulations of multiprotein complexes: Application to ubiquitin binding*, J. Mol. Biol., 2008, **375**, 1416-1433.
- 15 B. Różycki, M. Cieplak and M. Czjzek, *Large conformational fluctuations of the multi-domain xylanase Z of Clostridium thermocellum*, J. Struct. Biol., 2015, **191**, 68-75.
- 16 T.A. Leonard, B. Różycki, L.F. Saidi, G. Hummer and J.H. Hurley, *Crystal structure and allosteric activation of protein kinase C beta-II*, Cell, 2011, **144**, 55-66.

- 17 D.M. Francis, B. Różycki, D. Koveal, G. Hummer, W. Peti and R. Page, *Structural basis of p38 α regulation and specificity by hematopoietic tyrosine phosphatase*, Nature Chem. Biol., 2011, **7**, 916-924.
- 18 D.M. Francis, B. Różycki, A. Tortajada, G. Hummer, W. Peti and R. Page, *Resting and active states of the ERK2:HePTP complex*, J. Am. Chem. Soc., 2011, **133**, 17138-17141.
- 19 J. Schymkowitz, J. Borg, F. Stricher, R. Nys, F. Rousseau and L. Serrano, *The FoldX web server: an online force field*, Nucl. Acids Res., 2005, **33**, W382-388.
- 20 S. Miyazawa and R. L. Jernigan, *Residue-residue potentials with a favorable contact pair term and an unfavorable high packing density term, for simulation and threading*, J. Mol. Biol., 1996, **256**, 623-644.
- 21 M. Biasini, S. Bienert, A. Waterhouse, K. Arnold, G. Studer, T. Schmidt, F. Kiefer, T.G. Cassarino, M. Bertoni, L. Bordoli and T. Schwede, *SWISS-MODEL: modelling protein tertiary and quaternary structure using evolutionary information*, Nucl. Acids Res., 2014, **42**, W252-W258.
- 22 A. Fiser, R. Kihlman and A. Sali, *Modeling of loops in protein structures*, Protein Sci., 2000, **9**, 1753-1773.
- 23 M. Cieplak and T.X. Hoang, *Universality classes in folding times of proteins*, Biophys. J., 2003, **84**, 475-488.
- 24 M. Sikora, J.I. Sułkowska and M. Cieplak, *Mechanical strength of 17 134 model proteins and cysteine slipknots*, PLOS Comp. Biol., 2009, **5**, e1000547.
- 25 B. Różycki, Ł. Mioduszeński and M. Cieplak, *Unbinding and unfolding of adhesion protein complexes through stretching: Interplay between shear and tensile mechanical clamps*, Proteins: Struct. Funct. Bioinf., 2014, **82**, 3144-3153.
- 26 A.B. Poma, M. Chwastyk and M. Cieplak, *Polysaccharide-Protein Complexes in a Coarse-Grained Model*, J. Phys. Chem. B, 2015, **119**, 12028-12041.
- 27 D.M.A. Guerin, M.-B. Lascombe, M. Costabel, H. Souchon, V. Lamzin, P. Beguin and P.M. Alzari, *Atomic (0.94 Å) resolution structure of an inverting glycosidase in complex with substrate*, J. Mol. Biol., 2002, **316**, 1061-1069.
- 28 K. Wolek, A. Gomez-Sicilia and M. Cieplak, *Determination of contact maps in proteins: A combination of structural and chemical approaches*, J. Chem. Phys., 2015, **143**, 243105.
- 29 J. Tsai, R. Taylor, C. Chothia and M. Gerstein, *The packing density in proteins: Standard radii and volumes*, J. Mol. Biol., 1999, **290**, 253-266.
- 30 J.I. Kwiecinska and M. Cieplak, *Chirality and protein folding*, J. Phys. Cond. Mat., 2005, **17**, S1565-S1580.
- 31 T. Veitshans, D. Klimov and D. Thirumalai, *Protein folding kinetics: Timescales, pathways and energy landscapes in terms of sequence dependent properties*, Folding and Design, 1997, **2**, 1-22.
- 32 P. Szymczak and M. Cieplak, *Stretching of proteins in a uniform flow*, J. Chem. Phys., 2006, **125**, 164903.
- 33 W. Humphrey, A. Dalke and K. Schulten, *Vmd: Visual molecular dynamics*, J. Mol. Graph., 1996, **14**, 33-38.
- 34 J.C. Phillips, R. Braun, W. Wang, J. Gumbart, E. Tajkhorshid, E. Villa, et al., *Scalable molecular dynamics with NAMD*, J. Comput. Chem., 2005, **26**, 1781-1802.
- 35 A.D. MacKerell, D. Bashford, M. Bellott, R.L. Dunbrack, J.D. Evanseck, M.J. Field, et al., *All-atom empirical potential for molecular modeling and dynamics studies of proteins*, J. Phys. Chem. B, 1998, **102**, 3586-3616.
- 36 A.D. Mackerell, M. Feig and C.L. Brooks, *Extending the treatment of backbone energetics in protein force fields: Limitations of gas-phase quantum mechanics in reproducing protein conformational distributions in molecular dynamics simulations*, J. Comput. Chem., 2004, **25**, 1400-1415.
- 37 E.R. Hatcher, O. Guvench and A.D. Mackerell, *CHARMM additive all-atom force-field for acyclic polyalcohols, acyclic carbohydrates, and inositol*, J. Chem. Theory. Comput., 2009, **5**, 1315-1327.
- 38 O. Guvench, E.R. Hatcher, R.M. Venable, R.W. Pastor and A.D. Mackerell, *CHARMM additive all-atom force field for glycosidic linkages between hexopyranoses*, J. Chem. Theory Comput., 2009, **5**, 2353-2370.
- 39 O. Guvench, S.S. Mallajosyula, E.P. Raman, E.R. Hatcher, K. Vanommeslaeghe, et al., *CHARMM additive all-atom force field for carbohydrates derivatives and its utility in polysaccharides and carbohydrate-protein modeling*, J. Chem. Theory Comput., 2011, **7**, 3162-3180.
- 40 W.L. Jorgensen, J. Chandrasekhar and J.D. Madura, *Comparison of simple potential functions for simulating liquid water*, J. Chem. Phys., 1983, **79**, 926-935.
- 41 E. Papaleo, G. Saladino, M. Lambrugh, K. Lindorff-Larsen, F.L. Gervasio and R. Nussinov, *The Role of protein loops and linkers in conformational dynamics and allostery*, Chem. Rev., 2016, **116**, 6391-6423.
- 42 B. Różycki and E. Boura, *Large, dynamic, multi-protein complexes: a challenge for structural biology*, J. Phys. Cond. Mat., 2014, **26**, 463103.
- 43 J.A. Byun and G. Melacini, *Disordered Regions Flanking Ordered Domains Modulate Signaling Transduction*, Biophys. J., 2015, **109**, 2447-2448.
- 44 B. Ma, C.-J. Tsai, T. Haliloglu and R. Nussinov, *Dynamic allostery: linkers are not merely flexible*, Structure, 2011, **19**, 907-917.
- 45 M. Akimoto, R. Selvaratnam, E.T. McNicholl, G. Verma, S.S. Taylor and G. Melacini, *Signaling through dynamic linkers as revealed by PKA*, Proc. Natl. Acad. Sci. USA, 2013, **110**, 14231-14236.
- 46 I. Lucic, L. Truebestein and T.A. Leonard, *Novel Features of DAG-Activated PKC Isozymes Reveal a Conserved 3-D Architecture*, J. Mol. Biol., 2015, **428**, 121-141.